

# Assessment of a quantum phase-gate operation based on nonlinear optics

S. Rebić,\* C. Ottaviani, G. Di Giuseppe, D. Vitali, and P. Tombesi  
 Dipartimento di Fisica, Università di Camerino, I-62032 Camerino (MC), Italy  
 (Received 11 May 2006; published 1 September 2006)

We analyze in detail the proposal for a two-qubit gate for travelling single-photon qubits recently presented by Ottaviani *et al.* [Phys. Rev. A **73**, 010301(R) (2006)]. The scheme is based on an ensemble of five-level atoms coupled to two quantum and two classical light fields. The two quantum fields undergo cross-phase modulation induced by electromagnetically induced transparency. The performance of this two-qubit quantum phase gate for travelling single-photon qubits is thoroughly examined in the steady-state and transient regimes, by means of a full quantum treatment of the system dynamics. In the steady-state regime, we find a general trade-off between the size of the conditional phase shift and the fidelity of the gate operation. However, this trade-off can be bypassed in the transient regime, where a satisfactory gate operation is found to be possible, significantly reducing the gate operation time.

DOI: [10.1103/PhysRevA.74.032301](https://doi.org/10.1103/PhysRevA.74.032301)

PACS number(s): 03.67.Mn, 42.50.Gy, 42.65.-k

## I. INTRODUCTION

A promising system for quantum computation is to use single photons to encode quantum information [1]. This is due to the photon's robustness against decoherence and the availability of single-qubit operations. However, it is difficult to realize the necessary two-qubit operations since the physical interaction between photons is very small. Linear optics quantum computation [2] and nonlinear optical processes involving few photons have been proposed to circumvent this problem. The first is a probabilistic scheme implicitly based on the nonlinearity hidden in single-photon detectors, while the second is based on the enhancement of photon-photon interaction either in cavity QED configurations [3] or in dense atomic media exhibiting electromagnetically induced transparency (EIT) [4]. In this latter case, optical nonlinearities can be produced when EIT is disturbed, either by introducing additional energy level(s) [6,7], or by mismatching the probe and control field frequencies [8,9].

The scope of this paper is to assess the performance of a two-qubit quantum phase gate (QPG) for travelling single photon qubits [10–14], based on the cross-Kerr nonlinearity which is generated in a five-level atomic medium. In a QPG, one qubit gets a phase conditional to the other qubit state according to the transformation [15,16]  $|i\rangle_1 |j\rangle_2 \rightarrow \exp(i\phi_{ij}) |i\rangle_1 |j\rangle_2$  where  $\{i, j\} = 0, 1$  denote the logical qubit bases. This gate is universal when the conditional phase shift (CPS)

$$\phi = \phi_{11} + \phi_{00} - \phi_{10} - \phi_{01}, \quad (1)$$

is nonzero, and it is equivalent to a controlled-NOT (CNOT) gate up to local unitary transformations when  $\phi = \pi$  [15,16]. Most of the literature focused only on the evaluation of the CPS and on the best conditions for achieving  $\phi = \pi$  [10–14], while the gate fidelity, which is the main quantity for estimating the efficiency of a gate, has been evaluated in the full quantum limit in Ref. [17]. Here we provide the details of the calculation of the fidelity and the CPS of Ref. [17], which

showed the presence of a general *trade-off* between a large CPS and a gate fidelity close to one, hindering the QPG operation, in the stationary state. However, we shall see that this trade-off can be partially bypassed in the transient regime, which has never been considered before in EIT situations, still allowing a satisfactory gate performance.

The qubits are given by polarized single-photon wave packets with different frequencies, and the phase shifts  $\phi_{ij}$  are generated when these two pulses cross an atomic ensemble in a five-level  $M$  configuration (see Fig. 1). The population is assumed to be initially in the ground state  $|3\rangle$ . From this ground state, it could be excited by either the single-photon *probe* field, with central frequency  $\omega_p$  and coupling to transition  $|3\rangle \leftrightarrow |2\rangle$ , or by the single-photon *trigger* field, with central frequency  $\omega_t$  and coupling to transition  $|3\rangle \leftrightarrow |4\rangle$ . We assume that the five levels are Zeeman sublevels of an alkali atom, and that both pulses have a sufficiently narrow bandwidth. In this way, the Zeeman splittings can be chosen so that the atomic medium is coupled only to a given circular polarization of either the probe or trigger field, while it is transparent for the orthogonally polarized mode, which crosses the gas undisturbed [11]. As a consequence, the logical basis for each qubit practically coincides with the two lowest Fock states of the mode with the “right” polarization,  $|0_j\rangle$  and  $|1_j\rangle$  ( $j=p, t$ ), while the “wrong” polarization modes will be neglected from now on.

A classical pump field, with frequency  $\omega_1$  and Rabi frequency  $\Omega_1$ , couples to the transition  $|1\rangle \leftrightarrow |2\rangle$ , while a second

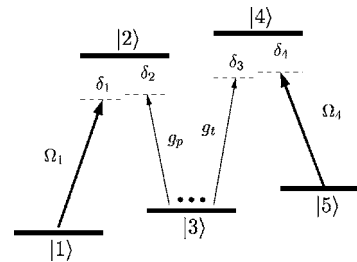


FIG. 1. Energy levels of the  $M$  scheme.  $\Omega_j$  are the Rabi frequencies of classical fields, while  $g_{p,t}$  denote couplings of the quantized probe and trigger fields to their respective transitions.  $\delta_j$  are the detuning of the fields from resonance.

\*Electronic address: [stojan.rebic@unicam.it](mailto:stojan.rebic@unicam.it)

classical pump field, with frequency  $\omega_4$  and Rabi frequency  $\Omega_4$ , couples to the transition  $|4\rangle \leftrightarrow |5\rangle$  (see Fig. 1). We consider a cylindrical, quasi-1D, atomic medium with the two classical pump beams propagating along its axis, collinear with the two quantum fields in order to avoid Doppler broadening. When the probe field is on two-photon resonance with the pump field with Rabi frequency  $\Omega_1$ , and the trigger field is on two-photon resonance with the pump field with Rabi frequency  $\Omega_4$ , the system exhibits EIT for probe and trigger simultaneously. This simultaneous EIT condition is achieved when

$$\delta_1 = \delta_2, \quad \delta_3 = \delta_4, \quad (2)$$

where the detunings  $\delta_j$  are defined by

$$E_2 - E_1 = \hbar \omega_1 + \hbar \delta_1, \quad (3a)$$

$$E_2 - E_3 = \hbar \omega_p + \hbar \delta_2, \quad (3b)$$

$$E_4 - E_3 = \hbar \omega_t + \hbar \delta_3, \quad (3c)$$

$$E_4 - E_5 = \hbar \omega_4 + \hbar \delta_4. \quad (3d)$$

A nonzero CPS occurs whenever a nonlinear cross-phase modulation (XPM) between probe and trigger is present. This cross-Kerr interaction takes place if the two-photon resonance condition is violated. For small frequency mismatch  $\epsilon_{12} = \delta_1 - \delta_2$  and  $\epsilon_{34} = \delta_3 - \delta_4$  (both chosen to be within the EIT window), absorption remains negligible and the cross-Kerr interaction between probe and trigger photons may be strong. The consequent CPS may become large, of the order of  $\pi$ , if the probe and trigger pulse interact for a sufficiently long time. If the two single photon pulses enter simultaneously the atomic medium, their interaction time  $t_{\text{int}}$  is optimized when the group velocities of the two pulses are equal, so that  $t_{\text{int}} = L/v_g$ , where  $v_g$  is the common group velocity of the pulses and  $L$  is the length of the gas cell. The inherent *symmetry* of the scheme guarantees perfect group velocity matching for probe and trigger whenever  $\delta_1 = \delta_4$ ,  $\delta_2 = \delta_3$  and  $g_p/\Omega_1 = g_t/\Omega_4$ , where  $g_j = \mu_j \sqrt{\omega_j/2\hbar \epsilon_0 V_j}$  ( $j=p,t$ ) is the coupling constant between the quantum mode with frequency  $\omega_j$  and mode volume  $V_j$ , and the corresponding transition with electric dipole moment  $\mu_j$ .

The importance of group velocity matching for achieving a significant nonlinear phase shift was first pointed out in Ref. [10], which suggested to use a mixture of two different atomic species to achieve this goal. The first kind of atoms generates XPM by means of a four-level  $N$  scheme [6], in which however only the probe field undergoes EIT and it is slowed down, while the second kind of atoms realizes a three-level  $\Lambda$  scheme able to slow down the trigger pulse. Group velocity matching is achieved by means of an accurate but difficult control of the atomic densities. A different way of achieving group velocity matching, but which is still asymmetric for probe and trigger has been proposed in Ref. [11], which employs a five-level  $M$  scheme similar to the one discussed here, but with a different atomic population distribution. In that case, the two group velocities can be tuned and made equal simply by tuning the frequencies and intensities of the two classical pump fields. Instead, Ref. [12]

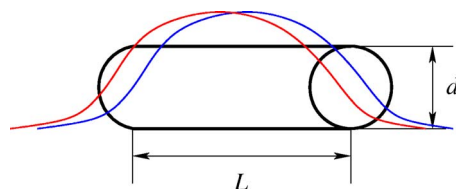


FIG. 2. (Color online) A schematic plot of the assumed single-photon pulse propagation through the gas cell of length  $L$  and diameter  $d$ . The pulse length is assumed to coincide with the cell length  $L$ , and the pulse waist  $w$  is assumed to be of order of cell diameter  $d$ .

considered a six-level scheme in which probe and trigger are affected by EIT and XPM in a symmetric fashion, so that the corresponding group velocities are equal by construction. The present proposal achieves group velocity matching just in the same way (see also Ref. [13], where a four-level tripod system, symmetric between probe and trigger, has been proposed for XPM).

The paper is organized as follows. In Sec. II we describe the model used in the remainder of the paper. Section III shows the results of a perturbative calculation for the CPS. These are used as a motivation to pass to a density matrix based calculation in Sec. IV, describing a QPG operation in a steady state. Then, the transient regime is explored in Sec. V, while in Sec. VI a scheme for the experimental verification of the QPG operation is discussed in detail. Conclusions are given in Sec. VII.

## II. MODEL

In this section, we present the model we have adopted for a full quantum description of the interaction of the two single-photon wave packets with the atomic medium possessing the level structure outlined in Fig. 1. To this end, we make the following two assumptions which, even though not simple to realize experimentally, are more technical than physical in nature:

(1) We assume perfect spatial mode matching between the input single-photon pulses entering the gas cell and the optical modes naturally excited by the driven atomic medium, and which are determined by the geometrical configuration of the gas cell and of the pump beams [18]. This allows us to describe the probe and trigger fields with the right polarization in terms of *single* travelling optical modes, with annihilation operators  $\hat{a}_{p,t}$ .

(2) We assume that the pulses are tailored in such a way that they simultaneously enter gas cell and completely overlap with it during the interaction (see Fig. 2). This means that their length (compressed inside a medium due to group velocity reduction) is of the order of the cell length  $L$  and their beam waist is of the order of the cell radius. In this way, the two pulses interact with *all*  $N_a$  atoms in the cell at once, and moreover, one can ignore spatial aspects of pulse propagation.

With these assumptions, and neglecting dipole-dipole interactions, the interaction picture Hamiltonian may be written as

$$\begin{aligned}
H = & \hbar \epsilon_{12} \hat{S}_{11} + \hbar \delta_2 \hat{S}_{22} + \hbar \delta_3 \hat{S}_{44} + \hbar \epsilon_{34} \hat{S}_{55} + \hbar \Omega_1 \sqrt{N_a} (\hat{S}_{21} \\
& + \hat{S}_{12}) + \hbar g_p \sqrt{N_a} (\hat{a}_p \hat{S}_{23} + \hat{S}_{32} \hat{a}_p^\dagger) + \hbar g_t \sqrt{N_a} (\hat{a}_r \hat{S}_{43} \\
& + \hat{S}_{34} \hat{a}_r^\dagger) + \hbar \Omega_4 \sqrt{N_a} (\hat{S}_{45} + \hat{S}_{54}), \quad (4)
\end{aligned}$$

where we have defined the collective atomic operators

$$\hat{S}_{kl} = \frac{1}{\sqrt{N_a}} \sum_{i=1}^{N_a} \sigma_{kl}^i, \quad k \neq l = 1, \dots, 5, \quad (5a)$$

$$\hat{S}_{kk} = \sum_i \sigma_{kk}^i, \quad (5b)$$

with  $\sigma_{kl}^j \equiv |k\rangle_i \langle l|$  being the operator switching between states  $k$  and  $l$  of the  $i$ th atom. The initial state of the system corresponds to a probe and a trigger single-photon pulse with generic polarization, simultaneously entering the medium in which all the atoms are initially in state  $|3\rangle$ . Since we consider only the polarization mode interacting with the medium, both for the probe and the trigger, the initial state can be written as

$$\begin{aligned}
|\psi_{\text{in}}\rangle = & \otimes_{i=1}^{N_a} (|3\rangle_i \otimes (c_{00}|0_p\rangle \otimes |0_t\rangle + c_{01}|0_p\rangle \otimes |1_t\rangle + c_{10}|1_p\rangle \otimes |0_t\rangle \\
& + c_{11}|1_p\rangle \otimes |1_t\rangle). \quad (6)
\end{aligned}$$

Due to the above assumptions, the passage of the two pulses through the atomic medium of length  $L$  corresponds to the time evolution of this state, for a time  $t_{\text{int}} = L/v_g$ , according to the master equation [5]

$$\begin{aligned}
\dot{\rho} = & -\frac{i}{\hbar} [H, \rho] + \sum_k \frac{\gamma_{kk}}{2} \sum_{j=1}^{N_a} (2\sigma_{kk}^j \rho \sigma_{kk}^j - \sigma_{kk}^j \rho - \rho \sigma_{kk}^j), \\
& + \sum_{kl} \frac{\gamma_{kl}}{2} \sum_{j=1}^{N_a} (2\sigma_{kl}^j \rho \sigma_{kl}^{j\dagger} - \sigma_{kl}^{j\dagger} \sigma_{kl}^j \rho - \rho \sigma_{kl}^{j\dagger} \sigma_{kl}^j), \quad (7)
\end{aligned}$$

including not only the coherent interaction described by the Hamiltonian of Eq. (4), but also the spontaneous emission from the excited states  $l=2, 4$  to the ground states  $k=1, 3, 5$  ( $\gamma_{kl}$  denotes the corresponding decay rate) and the dephasing of levels  $|k\rangle$ ,  $k=1, 2, 4, 5$ , with dephasing rate  $\gamma_{kk}$ . Typically the dephasing rates are much smaller than the decay rates,  $\gamma_{kl} \gg \gamma_{kk}$ ,  $\forall k, l$ .

Since the initial state of Eq. (6) contains at most two excitations, the coherent time evolution driven by Eq. (4) is simple and restricted to a finite-dimensional Hilbert space involving few symmetric collective atomic states. In fact, each component of the initial state of Eq. (6) evolves independently in a different subspace. The component with no photon is an eigenstate of  $H$  and does not evolve. The  $\otimes_{i=1}^{N_a} |3\rangle_i |0_p\rangle \otimes |1_t\rangle$  component evolves in a three-dimensional Hilbert space which it spans together with the two states  $|e_4^{(0,0)}\rangle$  and  $|e_5^{(0,0)}\rangle$ . Here, we have defined the symmetric collective states

$$|e_r^{(n_p, n_t)}\rangle = \frac{1}{\sqrt{N_a}} \sum_{i=1}^{N_a} |3_1, 3_2, \dots, r_i, \dots, 3_{N_a}\rangle \otimes |n_p\rangle \otimes |n_t\rangle, \quad (8)$$

where  $r=1, 2, 4, 5$ . In a similar fashion, the component with only one probe photon evolves in a three-dimensional Hilbert space spanned by the three states  $\otimes_{i=1}^{N_a} |3\rangle_i |1_p\rangle \otimes |0_t\rangle$ ,  $|e_1^{(0,0)}\rangle$  and  $|e_2^{(0,0)}\rangle$ . The component with one probe and one trigger photon evolves in the five-dimensional subspace spanned by the four collective states  $|e_1^{(0,1)}\rangle$ ,  $|e_2^{(0,1)}\rangle$ ,  $|e_4^{(1,0)}\rangle$ , and  $|e_5^{(1,0)}\rangle$  and the state  $\otimes_{i=1}^{N_a} |3\rangle_i |1_p\rangle \otimes |1_t\rangle$ .

Decoherence effects, and more specifically spontaneous emission from each atom complicates this dynamics. However, we are in the weak excitation limit where, for  $l \neq 3$ ,  $\langle \sigma_{ll}^j \rangle \approx N_a^{-1} \ll 1$ , as shown by the fact that the Hamiltonian dynamics involve only the symmetric atomic states of the form of Eq. (8). This limit allows a drastic simplification of the effective time evolution. Following Duan *et al.* [19], we can introduce Fourier transforms of the individual atomic operators  $s_{kl}^\mu = \sum_{j=0}^{N_a-1} \sigma_{kl}^j e^{ij\mu N_a} / \sqrt{N_a}$ , where  $s_{kl}^0 = \hat{S}_{kl}$  are the collective operators defined in Eq. (5a). The sum over the atoms in Eq. (7) then transforms to the sum over the collective atomic modes with index  $\mu$ . In the weak excitation limit, the operators  $s_{kl}^\mu$  approximately commute with each other. This means that they represent independent collective atomic modes, and one can trace over the  $\mu \neq 0$  modes, so that the spontaneous emission term in the master equation becomes

$$\sum_{kl} \frac{\gamma_{kl}}{2} (2\hat{S}_{kl} \rho \hat{S}_{kl}^\dagger - \hat{S}_{kl}^\dagger \hat{S}_{kl} \rho - \rho \hat{S}_{kl}^\dagger \hat{S}_{kl}), \quad (9)$$

where the sum is now over the six ‘‘collective’’ spontaneous decay channels only, each characterized by the *single-atom* decay rate  $\gamma_{kl}$ . A similar argument applies to the dephasing term in the master equation (7). In fact, if we restrict to the subspace of the symmetric collective states of Eq. (8) involving only single atomic excitations, we can approximate in the dephasing terms of the master equation,

$$\sum_k \gamma_{kk} \sum_{j=1}^{N_a} \sigma_{kk}^j \rho \sigma_{kk}^j \approx \sum_k \gamma_{kk} \hat{S}_{kk} \rho \hat{S}_{kk}, \quad (10)$$

where  $\hat{S}_{kk}$  is given by Eq. (5b). Using Eqs. (9) and (10), the master equation of Eq. (7) in the weak excitation limit becomes

$$\begin{aligned}
\dot{\rho} = & -\frac{i}{\hbar} [H, \rho] + \sum_k \frac{\gamma_{kk}}{2} (2\hat{S}_{kk} \rho \hat{S}_{kk} - \hat{S}_{kk} \rho - \rho \hat{S}_{kk}) \\
& + \sum_{kl} \frac{\gamma_{kl}}{2} (2\hat{S}_{kl} \rho \hat{S}_{kl}^\dagger - \hat{S}_{kl}^\dagger \hat{S}_{kl} \rho - \rho \hat{S}_{kl}^\dagger \hat{S}_{kl}), \quad (11)
\end{aligned}$$

that is, it involves only the operators of the collective atomic mode with index  $\mu=0$ . This actually means that the single photon probe and trigger pulses excite only a restricted number of collective atomic states, so that the atomic medium behaves as an effective *single* five-level atom, with a *collectively enhanced* coupling with the optical modes  $g_j \sqrt{N_a}$ , but

with single-atom decay rates  $\gamma_{kl}$ , dephasing rates  $\gamma_{kk}$ , Rabi frequencies  $\Omega_i$ , and detunings  $\delta_i$ .

Spontaneous emission causes the four independent Hilbert subspaces corresponding to the four initial state components to become coupled. Moreover, the ‘‘cross’’ decay channels  $|4\rangle \rightarrow |1\rangle$  and  $|2\rangle \rightarrow |5\rangle$  couple the above-mentioned collective states with six new states,  $|e_1^{(1,0)}\rangle, |e_2^{(1,0)}\rangle, |e_3^{(2,0)}\rangle$  (populated if  $\gamma_{41} \neq 0$ ), and  $|e_5^{(0,1)}\rangle, |e_4^{(0,1)}\rangle, |e_3^{(0,2)}\rangle$  (populated if  $\gamma_{25} \neq 0$ ). Therefore Eq. (11) actually describes dynamics in a Hilbert space of dimension 18, which we have numerically solved in order to establish the performance of the QPG. Notice that, due to the combined action of the cross-decay channels and of the Hamiltonian (4), the states  $|e_1^{(1,0)}\rangle, |e_2^{(1,0)}\rangle, |e_5^{(0,1)}\rangle$ , and  $|e_4^{(0,1)}\rangle$  are coupled also to *doubly excited* atomic collective states without photons which are neglected by our treatment. However, as we shall see below in the paper, a good QPG performance is possible only when spontaneous emission events are rare. Under this condition, the probability to populate these doubly excited atomic collective states during the atom-field interaction is completely negligible, and therefore our model based on the effective single five-level atom description provided by Eq. (11) is essentially correct.

In summary, the model outlined above relies on the single-photon nature of the excitations. In this case, the collective operators (5) effectively switch between the states making the superposition  $|\psi_{in}\rangle$  (6), and the symmetric collective states  $|e_r^{(n_p, n_t)}\rangle$  (8). This is central to the reasoning leading to the effective master equation (11).

To characterize the QPG operation, we calculate the CPS  $\phi$  of Eq. (1) and the *fidelity* of the gate. The accumulated CPS  $\phi$  as a function of the interaction time  $t_{int}$  is obtained by using the fact that the phase shifts  $\phi_{ij}$  of Eq. (1) are given by combinations of the phases of the off-diagonal matrix elements (in the Fock basis) of the reduced density matrix of the probe and trigger modes,  $\rho_f(t) = \text{Tr}_{atoms}[\rho(t)]$ .

The gate fidelity is given by [16]

$$\mathcal{F}(t) = \sqrt{\langle \psi_{id}(t) | \rho_f(t) | \psi_{id}(t) \rangle}, \quad (12)$$

where

$$\begin{aligned} |\psi_{id}(t)\rangle = & c_{00} \exp[i\phi_{00}(t_{int})] |0_p, 0_t\rangle + c_{01} \exp[i\phi_{01}(t)] |0_p, 1_t\rangle \\ & + c_{10} \exp[i\phi_{10}(t)] |1_p, 0_t\rangle + c_{11} \exp[i\phi_{11}(t)] |1_p, 1_t\rangle \end{aligned} \quad (13)$$

is the ideally evolved state from the initial condition (6), with phases  $\phi_{ij}(t)$  evaluated from  $\rho_f(t)$  as discussed above. The overbar denotes the average over all initial states (i.e., over the  $c_{ij}$ , see Poyatos *et al.* [20]). The above fidelity characterizes the performance of the QPG as a deterministic gate. However, one could also consider the QPG as a *probabilistic* gate, whose operation is considered only when the number of output photons is equal to the number of input photons. The performance of this probabilistic QPG could be experimentally studied by performing a conditional detection of the phase shifts, and it is characterized by the *conditional* fidelity  $\mathcal{F}^c(t)$ , which will be discussed in Sec. IV.

### III. PERTURBATIVE REGIME

The conditional fidelity is always larger than the unconditional one, but they become equal (and both approach 1) for an ideal QPG in which the number of photons is conserved and all the atoms remain in state  $|3\rangle$ . This ideal condition is verified in the limit of large detunings  $\delta_j \gg \gamma_{kj}$  so that spontaneous emission is significantly suppressed and can be neglected, and very small couplings  $g_j \sqrt{N_a} \ll \Omega_j$ . In this limit, each component of the initial state of Eq. (6) practically coincides with the dark state of the four independent Hamiltonian dynamics discussed in Sec. II. The system with the initial state containing zero probe and trigger photons does not evolve, i.e., stays in the initial state  $\otimes_{i=1}^{N_a} |3\rangle_i |0_p\rangle \otimes |0_t\rangle$  all the time.

The subsystem containing one probe and zero trigger photons as the initial state evolves according to a reduced three-dimensional Hamiltonian, which in the basis formed by the states  $\otimes_{i=1}^{N_a} |3\rangle_i |1_p\rangle \otimes |0_t\rangle, |e_2^{(0,0)}\rangle$  and  $|e_1^{(0,0)}\rangle$ , is given by

$$H_p = \begin{pmatrix} 0 & g_p \sqrt{N_a} & 0 \\ g_p \sqrt{N_a} & \delta_2 & \Omega_1 \\ 0 & \Omega_1 & \epsilon_{12} \end{pmatrix}. \quad (14a)$$

Similarly, the subsystem containing one trigger and zero probe photons as the initial state evolves according to a reduced three-dimensional Hamiltonian, which in the basis formed by the states  $\otimes_{i=1}^{N_a} |3\rangle_i |0_p\rangle \otimes |1_t\rangle, |e_4^{(0,0)}\rangle$  and  $|e_5^{(0,0)}\rangle$ , is given by

$$H_t = \begin{pmatrix} 0 & g_t \sqrt{N_a} & 0 \\ g_t \sqrt{N_a} & \delta_3 & \Omega_4 \\ 0 & \Omega_4 & \epsilon_{34} \end{pmatrix}. \quad (14b)$$

Finally, the subsystem containing initially one photon each in probe and trigger modes evolves according to a reduced five-dimensional Hamiltonian, which in the basis formed by the states  $|e_1^{(0,1)}\rangle, |e_2^{(0,1)}\rangle, \otimes_{i=1}^{N_a} |3\rangle_i |1_p\rangle \otimes |1_t\rangle, |e_4^{(1,0)}\rangle$ , and  $|e_5^{(1,0)}\rangle$ , is given by

$$H_{pt} = \begin{pmatrix} \delta_2 & \Omega_1 & g_p \sqrt{N_a} & 0 & 0 \\ \Omega_1 & \epsilon_{12} & 0 & 0 & 0 \\ g_p \sqrt{N_a} & 0 & 0 & g_t \sqrt{N_a} & 0 \\ 0 & 0 & 0 & \delta_3 & \Omega_4 \\ 0 & 0 & g_t \sqrt{N_a} & \Omega_4 & \epsilon_{34} \end{pmatrix}. \quad (14c)$$

The phase accumulation experienced by the various components of the quantum state of the fields will be proportional to the eigenvalues of these matrices. The four phase shifts  $\phi_{ij}$  can be evaluated as a fourth-order perturbation expansion of the eigenvalue corresponding to the dark state in each subspace, multiplied by the interaction time  $t_{int}$ . The CPS is then calculated as

$$\phi = (\lambda_{H_{pt}} - \lambda_{H_p} - \lambda_{H_t}) t_{int}, \quad (15)$$

where the  $\lambda$ 's denote the eigenvalues of the corresponding reduced Hamiltonian, with  $\lambda_{H_{pt}} \leftrightarrow \phi_{11}$ ,  $\lambda_{H_p} \leftrightarrow \phi_{10}$ ,  $\lambda_{H_t} \leftrightarrow \phi_{01}$ , and  $\phi_{00} = 0$ , in agreement with the general definition of Eq. (1). Following this procedure results in the following CPS:

$$\phi = \frac{g_p g_t N_a^2 t_{\text{int}}}{(\epsilon_{34} \delta_3 - \Omega_4^2)(\epsilon_{12} \delta_2 - \Omega_1^2)} \times \left( \frac{\epsilon_{34}(\epsilon_{12}^2 + \Omega_1^2)}{(\epsilon_{12} \delta_2 - \Omega_1^2)} + \frac{\epsilon_{12}(\epsilon_{34}^2 + \Omega_4^2)}{(\epsilon_{34} \delta_3 - \Omega_4^2)} \right). \quad (16)$$

This prediction is verified by the numerical solution of Eq. (11) in the limit of large detunings and small couplings. However the resulting CPS is too small, even for very long interaction times (i.e., long gas cells), for example, for  $g_{p,t}\sqrt{N_a}=0.5$  MHz,  $\epsilon_{12,34}=1.9$  MHz,  $\Omega_{1,4}=65$  MHz, and  $\delta_{2,3}=1.9$  GHz, we obtain a tiny CPS of only  $3 \times 10^{-4}$  radians when  $t_{\text{int}}=10^{-4}$  s, which corresponds to  $L \approx 30$  km. This is not surprising because this limit corresponds to a dispersive regime far from EIT. In this regime, transparency is achieved by means of a strong coupling field, producing a well-separated Autler-Townes doublet [5]. At the same time, the size of nonlinearity is small due to the extremely weak coupling of the quantized fields to their respective transitions. The results are, therefore, not different from those expected from XPM in a standard optical fiber [21]. Therefore, one must to explore the nonperturbative regime of larger couplings in order to exploit the low-noise, large-nonlinearity properties of EIT and achieve a satisfactory QPG operation.

#### IV. STEADY-STATE QPG OPERATION

A large amount of work exploring EIT-based nonlinear optical phenomena considers the steady state of a generic EIT-based system as being the natural state in which to predict and test different phenomena [6,7,9,11]. We shall see in this section that it is not possible to achieve a satisfactory QPG performance in such a steady-state regime.

In this section, we analyze the performance of the QPG at the steady state. To this end, we consider two different parameter regimes: (i) the regime of long interaction times, a natural extension of the perturbation analysis of Sec. III, and (ii) the regime of short interaction times, corresponding to a nonperturbative regime with strong atom-field coupling.

##### A. Long interaction time

Naturally extending the perturbative analysis, we solve the master equation (11), and show the results in Fig. 3. Figure 3 (left) shows the result for the conditional phase shift. Solid line has been calculated from the solution of Eq. (11), as explained in Sec. II. The dashed line is the benchmark solution, obtained from the eigenvalues of the associated Hamiltonian, by using Eq. (15). The eigenvalues of the Hamiltonians of Eqs. (14) have been calculated numerically for the set of parameters of Fig. 3.

It is evident that the benchmark solutions offers a reasonably good estimate for the size of the CPS. The exact dynamics driven by the master equation (11) presents an additional oscillatory behavior both on a short-time scale (transient processes), and on a long-time scale. The longer time scale comes from the fact that to induce the cross-Kerr nonlinearity, one must detune the fields away from the dark resonance. This detuning is very small and is seen in the oscillations on a long time scale. As both probe and trigger fields are de-

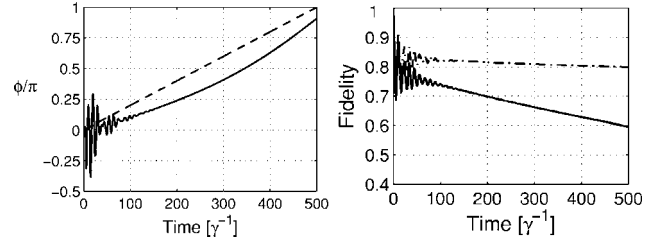


FIG. 3. Conditional phase shift (left) and the fidelity of Eq. (12) (right) as a function of the interaction time for  $N_a=10^6$ ,  $\delta_1=\delta_3=7.5\gamma$ ,  $\epsilon_{12}=\epsilon_{34}=0.05\gamma$ ,  $g_p=g_t=0.0011\gamma$ ,  $\Omega_1=\Omega_4=1.875\gamma$ , and  $\gamma_{kk}=\gamma_{ph}=10^{-3}\gamma$ ,  $\forall k$ . We have taken equal decay rates,  $\gamma_{21}=\gamma_{23}=\gamma_{25}=\gamma_{41}=\gamma_{43}=\gamma_{45}=\gamma/3$ , with  $\gamma=2\pi \times 6$  MHz. Left-hand side, solid line represents the phase shift, as calculated from the full master equation, while the dashed line gives the perturbative prediction of Eq. (16). Right-hand side, solid line is the unconditional gate fidelity  $\mathcal{F}(t)$ , while the dotted-dashed line is the conditional one,  $\mathcal{F}^c(t)$ .

tuned by the same amount, only one frequency of long-time oscillations is observed.

In Fig. 3 (right), fidelities (averaged over all possible two-qubit initial states) are shown in two cases. Both are calculated by using Eq. (12), but they differ in the way  $\rho_f(t)$  is defined. The solid line in Fig. 3 (right) refers to the *unconditional* fidelity  $\mathcal{F}(t)$ , which is calculated from Eq. (12) by taking  $\rho_f(t)=\text{Tr}_{\text{at}}[\rho(t)]$ , where  $\rho(t)$  is the solution of the master equation (11). The unconditional fidelity quantifies the performance of the QPG as a *deterministic* gate for single-photon qubits.

The dotted-dashed line in Fig. 3 (right) refers to the *conditional* fidelity  $\mathcal{F}^c(t)$ , which is evaluated according to Eq. (12), but with  $\rho_f(t)$  replaced by  $\rho_f^c(t)=\text{Tr}_{\text{at}}[|\psi_{n_j}(t)\rangle \langle \psi_{n_j}(t)|] / \langle \psi_{n_j}(t) | \psi_{n_j}(t) \rangle$ , where  $|\psi_{n_j}(t)\rangle$  is the (non-normalized) evolved atom-field state conditioned to the detection of no quantum jumps [22], i.e., of no photon loss by spontaneous emission. This fidelity can be measured by post-selecting those measurement results that conserve photon number, i.e., discarding those data sets where at least a photon from the initial two-qubit state has been lost to the environment. The conditional fidelity quantifies the performance of the QPG as a *probabilistic* two-qubit gate.

In Fig. 3, we have found at best a CPS of  $\sim \pi$  in correspondence with fidelities  $\mathcal{F}(t_{\text{int}})$  and  $\mathcal{F}^c(t_{\text{int}})$  equal to 60% and 80%, respectively. This is due to the general presence of a *trade-off between the size of the CPS and of the gate fidelity*, as well as to the atomic dephasing [23]. This is an important result of our paper, which actually holds true in *any* EIT-based nonlinear optics systems. In fact, both the conditional and the unconditional gate fidelity approach 1 in the limit of very small  $g_j$ , but this limit yields a CPS which becomes appreciable only for unrealistically long gas cells. For the parameters of Fig. 3,  $v_g=5.8 \times 10^6$ , which requires a cell of length  $v_g \times t_{\text{int}}=5.8 \times 10^6$  m/s  $\times$  (500/ $\gamma$ )  $\approx$  81 m. Therefore a larger CPS requires a larger ratio  $g_j\sqrt{N_a}/\Omega_j$ . This condition however increases the population of the collective atomic states  $|e_1^{(n_p, n_t)}\rangle$  and  $|e_3^{(n_p, n_t)}\rangle$  at the expense of the initial atomic state  $|3\rangle$ , thus unavoidably decreasing the gate fidelity. Similar conclusions hold for other options, such as in-

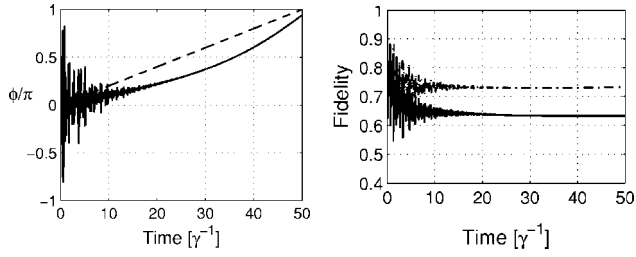


FIG. 4. Conditional phase shift (left) and the fidelity (right) as a function of the interaction time for  $N_a=10^8$ ,  $\delta_1=\delta_3=9.5\gamma$ ,  $\epsilon_{12}=\epsilon_{34}=0.2\gamma$ ,  $g_p=g_t=0.018\gamma$ ,  $\Omega_1=\Omega_4=19\gamma$ , and  $\gamma_{kk}=\gamma_{ph}=10^{-3}\gamma$ ,  $\forall k$ . We have taken equal decay rates,  $\gamma_{21}=\gamma_{23}=\gamma_{25}=\gamma_{41}=\gamma_{43}=\gamma_{45}=\gamma/3$ , with  $\gamma=2\pi\times 6$  MHz. Left-handed side, solid line represents the phase shift, as calculated from a density matrix, while the dashed line gives the eigenvalue solution. Right-hand side, solid line is the unconditional gate fidelity  $\mathcal{F}(t)$ , while the dotted-dashed line is the conditional one,  $\mathcal{F}^c(t)$ .

creased detunings  $\delta_j$ , or adjusting two-photon detunings  $\epsilon_{ij}$ . Therefore, just the pure coherent unitary evolution of the system, governed by the Hamiltonian of Eq. (4) causes this inherent trade-off.

### B. Short interaction time

To further illustrate our findings, we calculate the CPS and the gate fidelities in the range of parameters where the total interaction time is an order of magnitude smaller than in Sec. IV A. The CPS and the gate fidelities are calculated as described in Sec. IV A, and the results are shown in Fig. 4. To obtain a CPS of the order of  $\pi$  in a shorter interaction time ( $t_{\text{int}}\sim 50/\gamma$ ), we have assumed a larger ratio  $g_j\sqrt{N_a}/\Omega_j$ . The trade-off between the amount of accumulated nonlinear phase shift and the gate fidelity is now even more pronounced: we find at best a CPS of  $\sim\pi$  in correspondence with fidelities  $\mathcal{F}(t_{\text{int}})$  and  $\mathcal{F}^c(t_{\text{int}})$  equal to 65% and 73%, respectively. As expected, having a stronger atom-field coupling enhances the processes lowering the fidelity. The system ends up with a large CPS faster, but this is achieved with a final state in which the probability of losing the probe and trigger photons by spontaneous emission or within the atomic medium is no more negligible. We notice that in this short interaction time case dephasing does not have an appreciable effect, that is, the results without dephasing are indistinguishable from those with dephasing shown in Fig. 4, due to fact that dephasing rates in a dilute gas are typically much smaller than decay rates. The only possible way to circumvent this trade-off is to explore the transient regime, which will be discussed in the following section.

### V. QPG OPERATION IN TRANSIENT REGIME

In Sec. IV, we have found that the QPG operation of EIT-based nonlinear system in a steady state is plagued by the trade-off between the phase shift size and the gate fidelity. In an attempt to find favorable conditions for the QPG operation, we consider the transient regime, when  $\gamma t_{\text{int}}\lesssim 1$ . As discussed above, in order to accumulate a significant CPS in such a short time one must consider the strong coupling

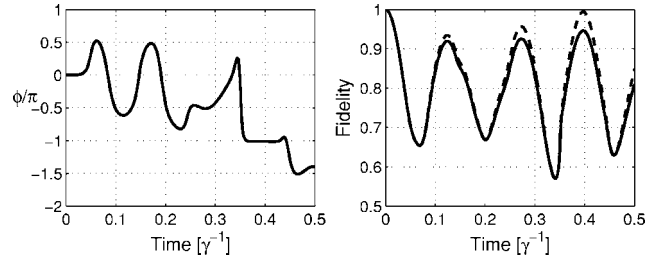


FIG. 5. Conditional phase shift (left) and the fidelity (right) of the QPG operation for  $N_a=10^6$ ,  $\delta_1=\delta_3=15\gamma$ ,  $\epsilon_{12}=\epsilon_{34}=0.01\gamma$ ,  $g_p=g_t=0.0022\gamma$ ,  $\Omega_1=\Omega_4=4\gamma$ , and  $\gamma_{kk}=\gamma_{ph}=10^{-3}\gamma$ ,  $\forall k$ . We have taken equal decay rates,  $\gamma_{21}=\gamma_{23}=\gamma_{25}=\gamma_{41}=\gamma_{43}=\gamma_{45}=\gamma/3$ , with  $\gamma=2\pi\times 6$  MHz. Right-hand side, the unconditional fidelity (solid) and conditional fidelity (dashed) are shown. See text for details.

regime with a large ratio  $g_j\sqrt{N_a}/\Omega_j$ . Therefore, the trade-off between fidelity and a large nonlinear interaction is present also in the transient regime. However, when  $g_j\sqrt{N_a}/\Omega_j$  is large, the transient dynamics is characterized by Rabi-type oscillations of the atomic populations and of the photon number, determining, as a consequence, coherent oscillations of the gate fidelity. In such a case one cannot exclude the existence of special values of the interaction time  $t_{\text{int}}$  corresponding to a maximum of the gate fidelity close to one, and at the same time, to a value of the CPS close to  $\pi$ .

We show that this fact is actually possible in Fig. 5, where we see that a CPS of  $\sim\pi$  radians is obtained in the transient regime for  $t_{\text{int}}\approx 0.4/\gamma\sim 10$  ns. At the same interaction time, the unconditional gate fidelity (Fig. 5, right, full line) is about 94%, while the conditional gate fidelity reaches the value of 99% (Fig. 5, right, dashed line). The conditional gate fidelity is obtained in correspondence with a success probability of the gate equal to 0.94, calculated from the norm of the Monte Carlo wave function [22]. The probe and trigger group velocities are calculated to be  $v_g\approx 3\times 10^6$  ms $^{-1}$ , yielding a gas cell length  $L=v_g t_{\text{int}}\approx 3.1$  cm. The value of  $g_j$  yields an interaction volume  $V\approx 2\times 10^{-3}$  cm $^3$ , corresponding to a gas cell diameter of about 330  $\mu\text{m}$  and to an atomic density  $N_a/V\approx 5\times 10^{10}$  cm $^{-3}$ .

To give a further example and to deepen our discussion of QPG performance and the CPS-fidelity trade-off, we now show the optimal results for the experimentally available pulses produced in the experiment of Darquié *et al.* [24] (see Fig. 6). The length of a pulse produced in Ref. [24] is 26 ns ( $\approx\gamma^{-1}$ ). The optimal parameters of Fig. 6 give the unconditional gate fidelity (Fig. 6, right, solid line) of 85%, while the conditional fidelity reaches 89% (Fig. 6, right, dotted-dashed line). The probe and trigger group velocities are calculated to be  $v_g\approx 1.51\times 10^6$  ms $^{-1}$ , yielding a gas cell length  $L=v_g t_{\text{int}}\approx 3.82$  cm. The value of  $g_j$  yields an interaction volume  $V\approx 10^{-1}$  cm $^3$ , corresponding to a gas cell diameter of about 910  $\mu\text{m}$  and to an atomic density  $N_a/V\approx 10^9$  cm $^{-3}$ . So, taking the longer wave packets (i.e., longer interaction times) means that the CPS-fidelity trade-off becomes increasingly important, and the top value of fidelity decreases slightly with respect to its optimal value.

Note how in both cases (Figs. 5 and 6) high values of fidelity could be obtained for values of CPS lower than  $\pi$

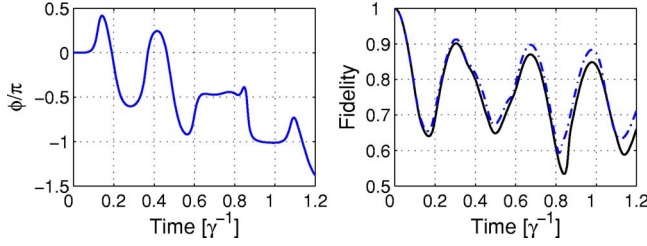


FIG. 6. (Color online) Conditional phase shift (left) and the fidelity (right) of a QPG operation for  $N_a=10^8$ ,  $\delta_2=\delta_3=6\gamma$ ,  $\epsilon_{12}=\epsilon_{34}=0.05\gamma$ ,  $g_p=g_t=0.0009\gamma$ , and  $\Omega_1=\Omega_4=\gamma$ . We have taken equal decay rates,  $\gamma_{21}=\gamma_{23}=\gamma_{25}=\gamma_{41}=\gamma_{43}=\gamma_{45}=\gamma/3$ . For  $^{87}\text{Rb}$ ,  $\gamma=2\pi\times 6$  MHz, giving the interaction time (i.e., pulse length) of  $\approx 25$  ns for  $|\phi|\approx\pi$ . Right-hand side, solid line denotes the deterministic fidelity, while dotted-dashed line denotes the conditional fidelity.

radians. This implies the possibility of the implementation of a *universal* quantum gate [15], which requires only  $\phi\neq 0$ .

A comment about this calculation of the common group velocity of the two wave packets,  $v_g$ , is in order. As mentioned earlier, EIT is stationary phenomenon, and in fact, the conventional  $v_g$  is a steady-state quantity which it is obtained from the susceptibility  $\chi$  according to

$$v_g = c \left[ 1 + \frac{1}{2} \text{Re}(\chi) + \frac{\omega_0}{2} \left( \frac{\partial \text{Re}(\chi)}{\partial \omega} \right)_{\omega_0} \right]^{-1} \quad (17)$$

( $\omega_0$  is the central frequency of wave packet), where the susceptibility of the  $j$ th field,  $\chi_j$  ( $j=p,t$ ), is evaluated from the associated steady-state atomic coherence  $\rho_j^{ss}$  as

$$\chi_j = \frac{N|\mu_j|^2}{V\hbar\epsilon_0\Omega_j} \rho_j^{ss}. \quad (18)$$

Instead, the above results are obtained in the transient regime where  $\gamma t_{\text{int}} < 1$ , and for this reason we have estimated the group velocity in a different way. We have evaluated the relevant time-dependent atomic coherence  $\rho_j(t)$  and the corresponding “instantaneous susceptibility”  $\chi_j(t)$  from the reduced atomic density matrix  $\rho_{\text{red}}(t) = \text{Tr}_{\text{fields}}[\rho(t)]$ , with  $\rho(t)$  being the solution of Eq. (11). The corresponding “instantaneous” group velocity  $v_g(t)$  has been then averaged over the time interval between 0 and  $t_{\text{int}}$ , providing in this way our estimate of the “transient” nonstationary group velocity of the single-photon wave packets. For the parameters of Fig. 6, this nonstationary  $v_g$  is approximately equal to  $c/100$  and it is about one order of magnitude smaller than the conventional  $v_g$  obtained from the steady-state susceptibility. This appreciable slowing down of the group velocity is a signature of a sort of “nonstationary” EIT process.

In order to verify that the nonstationary dynamics is really reminiscent of EIT, in the next section we compare these results with a numerical study of the three-level ladder atomic scheme (see Fig. 7), yielding XPM without EIT. Here we anticipate that we have found a smaller gate fidelity ( $\sim 78\%$ ) for a corresponding set of parameters, providing therefore further support to the presence of a moderate, nonstationary EIT process in the transient dynamics of our five-

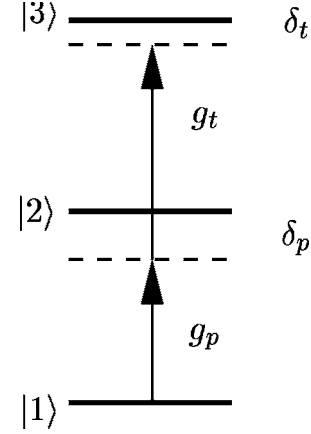


FIG. 7. Energy levels of the ladder scheme.  $g_{p,t}$  denote couplings of the quantized probe and trigger fields to their respective transitions.  $\delta_{p,t}$  are detunings of the probe and trigger fields from resonance.

level  $M$  scheme. This is because in the ladder scheme, the increase in the size of the nonlinearity (and thus the CPS) is accompanied by an increase of losses, unlike the case of any EIT-based scheme [6]. For this reason we also expect that our  $M$  scheme outperforms ladder scheme in the case of fully optimized fidelity for the  $\pi$  phase shift.

### A. The conventional three-level scheme

The atomic ladder scheme (see Fig. 7) is well known to exhibit XPM of the two fields involved [6]. In order to achieve a reasonable size of cross-phase shift, the detuning of the intermediate state  $\delta_p$  needs to be large. This minimizes spontaneous emission ( $\sim \gamma_2/\delta_p^2$ ), but also the size of XPM  $\sim 1/\delta_p^2$ .

In order to evaluate the XPM in a manner comparable to what we have done for the  $M$  scheme, we make similar assumptions and arrive at a description analogous to the one described in Sec. II. The Hamiltonian is now given by

$$H_3 = \hbar \delta_p \hat{S}_{22} + \hbar (\delta_p - \delta_t) \hat{S}_{33} + \hbar g_p \sqrt{N_a} (\hat{a}_p \hat{S}_{21} + \hat{S}_{12} \hat{a}_p^\dagger) + \hbar g_t \sqrt{N_a} (\hat{a}_t \hat{S}_{23} + \hat{S}_{32} \hat{a}_t^\dagger). \quad (19)$$

Following the same reasoning as in Sec. II, we arrive at the effective master equation (we neglect here atomic dephasing)

$$\dot{\rho} = \mathcal{L}_3 \rho = -\frac{i}{\hbar} [H_3, \rho] + \frac{\gamma_{21}}{2} (2\hat{S}_{12} \rho \hat{S}_{21} - \hat{S}_{21} \hat{S}_{12} \rho - \rho \hat{S}_{21} \hat{S}_{12}) + \frac{\gamma_{32}}{2} (2\hat{S}_{23} \rho \hat{S}_{32} - \hat{S}_{23} \hat{S}_{32} \rho - \rho \hat{S}_{23} \hat{S}_{32}), \quad (20)$$

where  $\gamma_{12}$  and  $\gamma_{23}$  denote the spontaneous emission rates from levels  $|2\rangle$  and  $|3\rangle$  to levels  $|1\rangle$  and  $|2\rangle$ , respectively, and the operators  $\hat{S}_{ij}$  denote collective atomic operators, in the spirit of Eq. (5a).

The results of the calculation of unconditional quantities are shown in Fig. 8, for a parameter regime comparable to that discussed in relation to Fig. 5 (see also Ref. [17]) for the five-level  $M$  scheme. The atoms are assumed to be in the



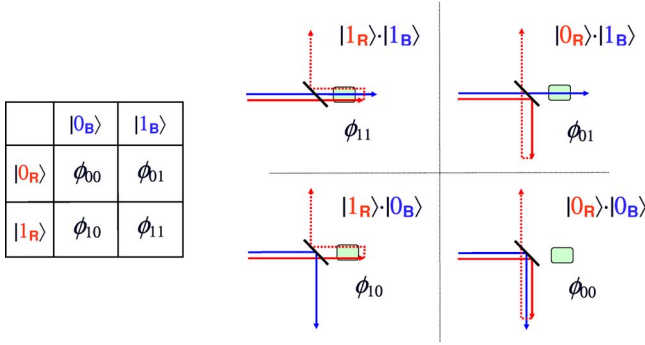


FIG. 10. (Color online) Truth table of the QPG for a logical basis of the qubits determined by the two lowest Fock states. On the right-hand side, diagrams corresponding to the probability amplitudes after the action of the BS and the FPs on the two-photons input state are shown.

99.9% (see the spectra in the right-hand inset of Fig. 9).

Since the frequency bandwidths of the two photons are well distinguished and the FPs filter out the trigger field, this apparatus determines an interferometer for the probe field only. The coincidence probabilities  $P(R, B1)$ , between  $D_R$  and  $D_{B1}$ , and  $P(R, B2)$ , between  $D_R$  and  $D_{B2}$ , post-select the events in which the trigger photon is. In this case the coincidence probabilities are equal and given by

$$P(R, B1) = P(R, B2) = [1 + \cos \Phi]/8, \quad (21)$$

where  $\Phi$  represents the phase difference due to the different optical paths of the two arms experienced by the probe. In arm 2 a delay line (DL) is added to compensate the difference in the optical path and to scan for the interference pattern. In the left-hand inset of Fig. 9 Sagnac-type version of the interferometer is shown, which allows for an auto-compensation of the optical path delay as the two arms coincide.

When an EIT-based XPM system is considered in one arm, say arm 1, a nonlinear contribution to the phase is added by the QPG, whether the trigger photon is present in the arm 1 or not. The XPM requires two intense classical fields resonant to the  $D_2F=1 \rightarrow F'=1$  (384.232 THz) and  $D_1F=1 \rightarrow F'=1$  (377.235 THz),  $\sigma^-$  circularly polarized tuner field ( $\alpha_t, \Omega_t$ ), and  $\sigma^+$  circularly polarized coupling field ( $\alpha_c, \Omega_c$ ), respectively. The coincidence probabilities  $P(R, B1)$ , between  $D_R$  and  $D_{B1}$ , and  $P(R, B2)$ , between  $D_R$  and  $D_{B2}$ , enable post-selection of the events in which the trigger photon is in the arm 2 and hence the interference pattern is given by Eq. (21). Instead a nonlinear contribution to the phase is expected when detections on  $D_R$  are post selected by the detection on  $D_{B2}$ . Figure 10 represents the diagram of the four amplitude probabilities after the action of the BS and the FPs on the two-photons state. The nonlinear phase  $\phi_{11}$  is added only to the first diagram.

According to the truth-table and the amplitudes of Fig. 10, the coincidence probabilities can be evaluated to be

$$P(R, B1) = [1 + \cos(\tilde{\Phi} + \phi)]/8, \quad (22)$$

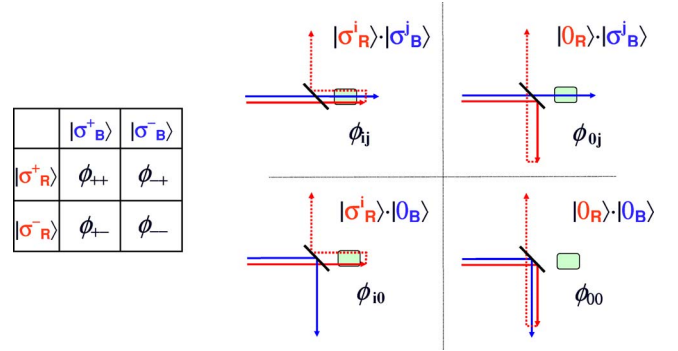


FIG. 11. (Color online) Truth table of the QPG for a logical basis of the qubits determined by orthogonal circular polarization basis. On the right-hand side the diagrams corresponding to the probability amplitudes after the action of the BS and the FPs on the two-photons input state.

$$P(R, B2) = [1 + \cos \tilde{\Phi}]/8. \quad (23)$$

with  $\tilde{\Phi} = \Phi + (\phi_{10} - 2\phi_{00} + \phi_{+0})$ .  $\phi_{+0}$  is the phase due to the probe photon reflected in arm 1 with “wrong”  $\sigma^+$  circular polarization. The phases  $\phi_{10}$  and  $\phi_{00}$  have been introduced in Eq. (1) as well as the conditional phase shift  $\phi = \phi_{11} - \phi_{01} - \phi_{10} + \phi_{00}$  of the QPG. The phase difference between the two interference patterns determined by the two coincidence probabilities determines univocally the value of  $\phi$ . In the case of an ideal QPG for which  $\phi = \pi$  the two coincidence probabilities have opposite phases.

*Polarization logical basis:* The previous proposal indirectly tests the QPG based on the XPM detecting the nonlinear phase shift by a Michelson interferometer and coincidence measurements. A direct measurement of the truth table or a test on a general qubit state requires a control and measurement of a superposition of vacuum and one photon state. While the generation of a superposition of vacuum and single photon state has been already achieved [24], the measurement of such a superposition requires also a homodyne measurement [25,26]. However a logical basis for the qubits can be chosen as the circular polarization basis of the probe and trigger photons. A test of the QPG will then require the detection of both photons thus avoiding a problematic production and detection of Fock state superpositions.

The experimental setup is the same as in Fig. 9, but the qubits are now encoded in the polarization of the input two-photon state.

According to the truth-table and the amplitudes in Fig. 11 it is possible to derive the coincidence probabilities  $P(R_i, B1_j)$  and  $P(R_i, B2_j)$ , with  $i, j = \{+, -\}$ , as

$$P(R_i, B1_j) = [1 + \cos(\tilde{\Phi} + \bar{\phi}_{ij})]/8, \quad (24)$$

$$P(R_i, B2_j) = [1 + \cos \bar{\Phi}]/8. \quad (25)$$

with  $\bar{\Phi} = \Phi + (\phi_{i0} - 2\phi_{00} + \phi_{(i\oplus 1)0})$ , where  $i \oplus 1$  is the sum mod 2. The phase  $\bar{\phi}$  is now given as  $\bar{\phi}_{ij} = \phi_{ij} - \phi_{i0} - \phi_{0j} + \phi_{00}$ , where  $\phi_{i0}$  is the phase due to the EIT for the probe photon with polarization  $i$  and no trigger photon

present, and the same meaning for the other phases. Note that for  $i=j=-' \equiv 1'$  one obtains the previous expression for the QPG phase in the logical Fock-state basis. Four possible choices of the probe and trigger polarizations determine the phases

$$\begin{aligned}\bar{\phi}_{--} &= \phi_{--} - \phi_{-0} - \phi_{0-} + \phi_{00}, \\ \bar{\phi}_{-+} &= \phi_{-+} - \phi_{-0} - \phi_{0+} + \phi_{00}, \\ \bar{\phi}_{+-} &= \phi_{+-} - \phi_{+0} - \phi_{0-} + \phi_{00}, \\ \bar{\phi}_{++} &= \phi_{++} - \phi_{+0} - \phi_{0+} + \phi_{00},\end{aligned}\quad (26)$$

which satisfies the relation  $\bar{\phi}_{--} - \bar{\phi}_{+-} - \bar{\phi}_{-+} + \bar{\phi}_{++} = \phi_{--} - \phi_{+-} - \phi_{-+} + \phi_{++} = \phi$ . In the case of an ideal EIT for which  $\phi_{+0} = \phi_{0+} = \phi_{++} = \phi_{00}$ ,  $\phi_{-+} = \phi_{-0} = \phi_R$ , and  $\phi_{+-} = \phi_{0-} = \phi_B$ , where  $\phi_{A,B}$  are the phases acquired by the single photons, we have  $\bar{\phi}_{--} = \phi$ , and  $\bar{\phi}_{-+} = \bar{\phi}_{+-} = \bar{\phi}_{++} = 0$ . In a way the phases between the two coincidence interference patterns allow a measurement of the QPG phases in the diagonal basis, i.e., in the single qubit states for which the only nonzero phase shift is the conditional phase shift  $\phi$  of the QPG.

*General polarization qubit input states:* The polarization logical basis allows for a direct observation of coherence and production of entanglement as necessary conditions for a QPG. Assume that the information is encoded in the polarization state of two photons, and then sent into the EIT-based XPM system for QPG, as shown in Fig. 12. The output photons, as shown in Fig. 12, are split by a dichroic mirror (a tilted FP cavity with the same parameters as before) and then collected in two APDs ( $D_R$  and  $D_B$ ) for coincidence counting. In front of each detector a tomographic system [27] constituted by a QWP, HWP and a PBS, is placed for the complete reconstruction of the polarization state of the output, thus providing the information on coherence properties of the gate. It has also been shown [3] that an input state for the QPG given by  $\{[(|\sigma_R^+\rangle + |\sigma_R^-\rangle) \otimes (|\sigma_B^+\rangle + |\sigma_B^-\rangle)]\}/2$  can quantify the entanglement of the output state, for which the CHSH inequality is  $2\sqrt{1 + \sin^2 \phi}$  where 2 is the upper classical limit.

## VII. CONCLUSION

In conclusion, our study shows that the implementation of efficient EIT-based nonlinear two-qubit gates for travelling single photons is possible, even though experimentally challenging. The main limitation is due to the existence of a

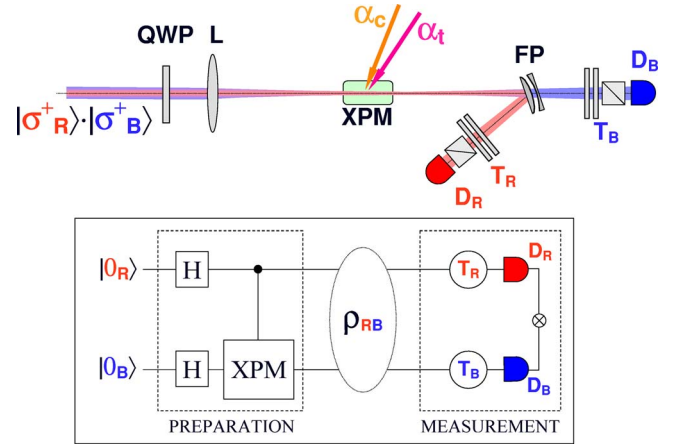


FIG. 12. (Color online) Scheme of the proposed experiment for a complete characterization of the QPG. Two photons in the  $\sigma^+$  polarization state (logical state  $|0_R\rangle \otimes |0_B\rangle$ ) are transformed by a QWP, corresponding to two Hadamard single-qubit gates, and then to the XPM medium (QPG). A Fabry-Perot cavity with the same parameter as before transmits the trigger photon and reflect the probe to two tomographic measurement systems ( $T_{R,B}$ ) and detected by APDs.

trade-off between the size of the CPS and the fidelity of the gate, limiting the achievable gate fidelity in the stationary regime, but which can be partially bypassed in the transient regime. Since this trade-off is a general consequence of the coherent interaction between the atomic medium and the single-photon wave packets, we expect that these considerations apply to all EIT-based crossed-Kerr schemes [10,11], regardless the specific level scheme considered. Instead, this consideration does not apply to situations where the nonlinearity comes from independent processes (e.g., collisions or dipole-dipole interactions) [14], nor the similar solid-state based processes [28].

## ACKNOWLEDGMENTS

This work has been partly supported by the European Commission through FP6/2002/IST/FETPI SCALA: ‘Scalable Quantum Computing with Light and Atoms’, Contract No. 015714, CONQUEST network, Contract No. MRTN-CT-2003-505089 and under the Integrated Project Qubit Applications (QAP) funded by the IST, Contract No. 015848. One of the authors (G.D.G.) also acknowledges financial support from the Ministero della Istruzione, dell’Università e della Ricerca (Grants Nos. PRIN-2005024254 and FIRB-RBAU01L5AZ).

- [1] I. L. Chuang and Y. Yamamoto, Phys. Rev. A **52**, 3489 (1995).  
 [2] E. Knill, R. Laflamme, and G. J. Milburn, Nature (London) **409**, 46 (2001).  
 [3] Q. A. Turchette, C. J. Hood, W. Lange, H. Mabuchi, and H. J. Kimble, Phys. Rev. Lett. **75**, 4710 (1995); A. Rauschenbeutel,

- G. Nogues, S. Osnaghi, P. Bertet, M. Brune, J. M. Raimond, and S. Haroche, *ibid.* **83**, 5166 (1999).  
 [4] E. Arimondo, in *Progress in Optics XXXV*, edited by E. Wolf (Elsevier, Amsterdam, 1996); S. E. Harris, Phys. Today **50**(7), 36 (1997); M. D. Lukin and A. Imamoglu, Nature (London)

- 413**, 273 (2001).
- [5] M. Fleischhauer, A. Imamoglu, and J. Marangos, *Rev. Mod. Phys.* **77**, 633 (2005).
- [6] H. Schmidt and A. Imamoglu, *Opt. Lett.* **21**, 1936 (1996).
- [7] H. Wang, D. Goorskey, and M. Xiao, *Phys. Rev. Lett.* **87**, 073601 (2001); H. Kang and Y. Zhu, *ibid.* **91**, 093601 (2003).
- [8] J.-F. Roch, K. Vigneron, P. Grelu, A. Sinatra, J. P. Poizat, and P. Grangier, *Phys. Rev. Lett.* **78**, 634 (1997); P. Grangier, D. F. Walls, and K. M. Gheri, *Phys. Rev. Lett.* **81**, 2833 (1998).
- [9] A. B. Matsko, I. Novikova, M. S. Zubairy, and G. R. Welch, *Phys. Rev. A* **67**, 043805 (2003); A. B. Matsko, *Opt. Lett.* **28**, 96 (2003); A. D. Greentree, D. Richards, J. A. Vaccaro, A. V. Durrant, S. R. de Echaniz, D. M. Segal, and J. P. Marangos, *Phys. Rev. A* **67**, 023818 (2003).
- [10] M. D. Lukin and A. Imamoglu, *Phys. Rev. Lett.* **84**, 1419 (2000).
- [11] C. Ottaviani, D. Vitali, M. Artoni, F. Cataliotti, and P. Tombesi, *Phys. Rev. Lett.* **90**, 197902 (2003).
- [12] D. Petrosyan and G. Kurizki, *Phys. Rev. A* **65**, 033833 (2002).
- [13] S. Rebić, D. Vitali, C. Ottaviani, P. Tombesi, M. Artoni, F. Cataliotti, and R. Corbalan, *Phys. Rev. A* **70**, 032317 (2004); D. Petrosyan and Y. P. Malakyan, *ibid.* **70**, 023822 (2004).
- [14] M. Mašalas and M. Fleischhauer, *Phys. Rev. A* **69**, 061801(R) (2004); I. Friedler, G. Kurizki, and D. Petrosyan, *ibid.* **71**, 023803 (2005); A. Andrè, M. Bajcsy, A. S. Zibrov, and M. D. Lukin, *ibid.* **94**, 063902 (2005).
- [15] S. Lloyd, *Phys. Rev. Lett.* **75**, 346 (1995).
- [16] M. A. Nielsen and I. L. Chuang, *Quantum Computation and Quantum Information* (Cambridge University Press, Cambridge 2000).
- [17] C. Ottaviani, S. Rebić, D. Vitali, and P. Tombesi, *Phys. Rev. A* **73**, 010301(R) (2006).
- [18] L.-M. Duan, J. I. Cirac, and P. Zoller, *Phys. Rev. A* **66**, 023818 (2002).
- [19] L. M. Duan, M. D. Lukin, J. I. Cirac, and P. Zoller, *Nature (London)* **414**, 413 (2001); J. I. Cirac, L. Duan, and P. Zoller, in *Experimental Quantum Computation and Information*, edited by F. De Martini and C. Monroe (IOS Press, Amsterdam 2002).
- [20] J. F. Poyatos, J. I. Cirac, and P. Zoller, *Phys. Rev. Lett.* **78**, 390 (1997).
- [21] G. P. Agrawal, *Nonlinear Fiber Optics*, 3rd ed. (Academic, London, 2001).
- [22] H. J. Carmichael, *An Open Systems Approach to Quantum Optics*, Lecture Notes in Physics (Springer, Berlin, 1993).
- [23] Without the dephasing, steady-state fidelities reach the values of 77% and 83% for unconditional and conditional cases, respectively.
- [24] B. Darquié, M. P. A. Jones, J. Dingjan, J. Beugnon, S. Bergamini, Y. Sortais, G. Messin, A. Browaeys, and P. Grangier, *Science* **309**, 454 (2005).
- [25] A. Zavatta, S. Viciani, and M. Bellini, *Science* **306**, 660 (2004).
- [26] S. A. Babichev, B. Brezger, and A. I. Lvovsky, *Phys. Rev. Lett.* **92**, 047903 (2004).
- [27] D. F. V. James, P. G. Kwiat, W. J. Munro, and A. G. White, *Phys. Rev. A* **64**, 052312 (2001).
- [28] J. J. Longdell, M. J. Sellars, and N. B. Manson, *Phys. Rev. Lett.* **93**, 130503 (2004); E. Fraval, M. J. Sellars, and J. J. Longdell, *ibid.* **92**, 077601 (2004); J. J. Longdell, E. Fraval, M. J. Sellars, and N. B. Manson, *ibid.* **95**, 063601 (2005); E. Fraval, M. J. Sellars, and J. J. Longdell, *ibid.* **95**, 030506 (2005).